Turbulence Induced Cloud Voids: Observation and Interpretation

Katarzyna Karpinska[1], Jonathan F.E. Bodenschatz[2], Szymon P. Malinowski[1], Jakub L. Nowak[1],
Steffen Risius[2], Tina Schmeissner[4], Raymond A. Shaw[3], Holger Siebert[4], Hengdong Xi[2], Haitao Xu[2],
and Eberhard Bodenschatz[2]

[1]Institute of Geophysics, Faculty of Physics, University of Warsaw, Warsaw, Poland
[2]Max Planck Institute for Dynamics and Self-Organization, Goetingen, Germany
[3]Michigan Technological University, Houghton, Michigan, USA
[4]Leibniz Institute for Tropospheric Research, Leipzig, Germany

Correspondence: S. P. Malinowski (malina@fuw.edu.pl)

Abstract. The phenomenon of "cloud voids", i.e., elongated volumes inside a cloud that are devoid of droplets, was observed
with laser sheet photography in clouds at a mountain-top station. Two experimental cases, similar in turbulence conditions yet
with diverse droplet size distributions and cloud void prevalence, are reported. A theoretical explanation is proposed based on
the study of heavy inertial sedimenting particles inside a Burgers vortex. A general conclusion regarding void appearance is

5   drawn from theoretical analysis. Numerical simulations of polydisperse droplet motion with realistic vortex parameters and
Mie scattering visual effects accounted for can explain the presence of voids with sizes similar to that of the observed ones.
Preferential concentration and sorting effects in a vortex tube are discussed for reasonable cloud conditions.

Copyright statement. TEXT

1   Introduction

10   The dynamics of heavy inertial particles in turbulent flow is a universal problem that appears in astrophysics, oceanography,
engineering and atmospheric sciences. In particular, in cloud physics, deeper understanding of the interaction between atmo-
spheric turbulence and cloud droplets is seen as a potential answer to many important questions (Bodenschatz et al. (2010)).
Over the years, there has been considerable speculation about the possible role of coherent, long-lived vortex structures in cloud
turbulence and microphysical processes, including both condensation growth and collision-coalescence growth (see Tennekes

15   and Woods (1973), Maxey and Corrsin (1986), Shaw et al. (1998), Shaw (2000), Markowicz et al. (2000), Hill (2005)). This
paper describes the first experimental observation of a phenomenon we refer to as "cloud voids" - cylindrical volumes devoid
of droplets recorded in real clouds - and is focused on determining whether inertially induced voids indeed occur in clouds due
to the presence of strong vortex structures.

20   Vortex tubes, sometimes called "worms", are severely intermittent, coherent, elongated and long-lasting structures character-
istic of high Reynolds number turbulent flows (e.g. Mouri et al. (2000)). Past theoretical and experimental studies lack general

conclusions about their characteristic time and length scales, intensity and appearance in turbulence. In particular, most of the research was conducted under conditions different from multiscale atmospheric turbulence. Statistical analysis based on such research (see e.g. Jiménez et al. (1993), Belin et al. (1999), Pirozzoli (2012)) showed that Burgers vortex core size δ (defined later in Eq. 2), scales roughly with the Kolmogorov length scale η:

$$\delta = m\eta \tag{1}$$

and that m has a distribution ranging from a few to a few tens with its mean around $m = 4$. Moisy and Jimenez (2004) analyzing DNS instant velocity fields propose that vorticity structures' geometrical aspect ratios evolve towards long tubes (1:1:10) with increasing vorticity threshold. What is more they show that these structures concentrate into clusters of the size in inertial range of scales. This implies the presence of large-scale organization of the small-scale intermittent structures. In the study by Biferale et al. (2000), statistics of vortex filament lifetime for a low Taylor microscale Reynolds number Re_λ indicate that the maximum lifetime is on the order of the integral timescale, whereas its mean scales with the Kolmogorov timescale. Numerical experiments described in Tanahashi et al. (2008) suggest that there is a relation between root mean square velocity fluctuations and the circulation parameter Γ of a vortex tube modeled as a Burgers vortex.

Previous efforts to study dynamics of heavy, inertial particles in vortices were made by simulating droplet trajectories in a prescribed velocity field for several simple single vortex models. Such research for the simplest model of a line vortex with stretching was conducted by Markowicz et al. (2000) with limitation to horizontally oriented vortices. In order to better understand the problem of cloud droplet dynamics in atmospheric conditions the same model but with arbitrary gravity alignment was studied by Karpinska and Malinowski (2014). Another model, free from the problem of unrealistic singularity on the vortex axis, is a Burgers vortex with stretching. It is commonly seen as a very good approximation of a real vortex tube (Neu (1984), Jimenez and Wray (1998)). The specific features of droplet motion for monodisperse droplets in a Burgers vortex were examined by Hill (2005) for horizontal alignment and by Marcu et al. (1995) for arbitrary alignment with respect to gravity.

In this paper we describe the serendipitous observation of numerous, isolated voids in clouds, while conducting measurements at a mountain-top station. The voids were visually striking and generated great excitement from the scientific team. Here, we present direct, 2D observations of the distinct types of patterns of clear air in clouds, along with accompanying turbulence and cloud microphysical measurements. We pose the question of whether the observed cloud voids are consistent with inertial droplet response to turbulence under atmospheric conditions. To answer this question, analysis of the particle dynamics in a Burgers vortex is further developed for the heavy sedimenting polydisperse case and the model is interpreted in the context of the observations.

The paper is structured as follows. Section 2 describes the measurement method and analysis of experimental data that shows the phenomenon of cloud voids. Section 3 presents relevant features of single droplet trajectories in a vortex tube model. Section 4 continues the analysis of droplet motion in a vortex to define the conditions of cloud void emergence. Section 5 describes a

method of finding simulation parameters corresponding to observed cloud voids, and Sect. 6 presents void simulation results. Section 7 incorporates the discussion and conclusions.

2   Experimental Evidence

Intriguing structures inside clouds, as presented in Fig. 1, were recorded by means of laser sheet photography during observa-
5   tions performed on 27 and 29 August 2011 at Umweltforschungsstation Schneefernerhaus (UFS) on the slopes of Mt. Zugspitze in the German Alps. Each time, the cloud event lasted for several hours. For a description of the observatory and characterization of the cloud and turbulence conditions on-site, see Risius et al. (2015) and Siebert et al. (2015). Authors of these papers showed that turbulence and cloud microphysical properties at the measurement site are quite reasonable representations of measurements made in 'free' clouds away from the surface.

10   Clouds were illuminated by a laser sheet created with a frequency-doubled high-power Nd:YAG laser (532 nm, 45 W). The sheet was set either vertical or oblique with respect to gravity. The angle between the laser sheet plane and camera recording plane in the oblique case was chosen to increase the scattering intensity on droplets and falls within the range of 30-40 degrees. The laser sheet in the observation region was around 50 cm wide and 1 cm thick. Images covering the approximately 2 m long section of the sheet at a distance approximately 10 m from the source were taken with a Nikon D3S DSLR 12 Mpix camera.

Laser sheet photography was accompanied by high-resolution measurements of small-scale turbulence and cloud micro-physics, as described in Siebert et al. (2015). Flow turbulence was measured by 3D ultrasonic anemometers operated at 10 Hz, from which the velocity structure functions were calculated using Taylor's frozen-flow hypothesis, and the energy dissipation rates were determined using inertial range scaling. Droplet size was measured by a PDI probe (Chuang et al., 2008) mounted
20   approximately 6 m down from the camera level. Figure 2 presents the measurement set-up and recorded size spectra of droplets. Droplet and turbulence measurements are summarized in the Table 1. The mean values refer to 30-minute long record corresponding to the camera acquisition series.

Two kinds of events in which droplet spatial distribution is visibly inhomogeneous were distinguished in the collected im-
25   ages. The first kind was characterized by an irregular interface separating clear-air and cloudy-air volumes and/or cloudy volumes of visibly different properties over a wide range of spatial scales (panel b) in Fig. 1). Inhomogeneities of the second type, present within the cloudy volumes, were called cloud voids in "Swiss cheese" clouds. The word "cloud holes" is avoided because it is commonly used referring to the cloud-free regions occurring in stratocumulus decks, as described for example in (Gerber et al., 2016). They were smaller (a few centimeters scale), the interface was usually blurry (see panels a) and c) in Fig.
30   1) and the shapes of clear-air regions were often close to round or elliptic (see magnified voids in Fig. 3). Inhomogeneities of the first kind are argued to be created in the process of cloud – clear-air mixing (Warhaft, 2000). In contrast, in some series of images and movies, the shape of the recorded tracks of cloud droplets suggest the following cloud void origin hypothesis: they result from interactions between inertial, heavy cloud droplets and small-scale vortices present in a turbulent cloud.
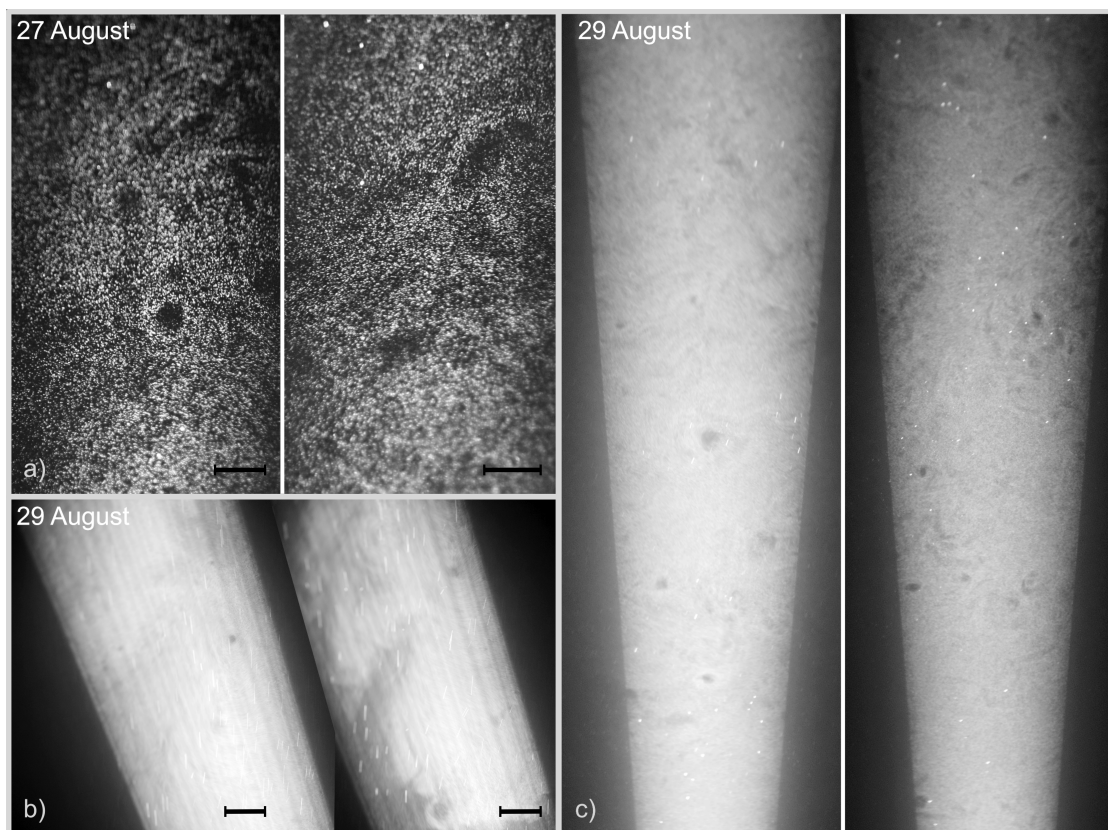
Figure 1. Examples of cloud voids observed at the UFS station with various camera-laser configurations. Pictures taken on 27 August (panel a) were chosen to estimate cloud void sizes. The ones recorded on 29 August evening (panel b) show the difference between inhomogeneities produced by cloud voids and those resulting from the mixing with clear air at the cloud edge. Other pictures from 29 August (panel c) suggest that the voids can be quite frequent in the sample volume. Bright spots and lines are due to presence of larger precipitation particles. 10 cm long segment is shown to represent spatial scale assumed in the void size calculation. For more details, see the movies attached in the supplementary materials.

Comparison of the two described cases becomes straightforward when conducted on the basis of the movies in the database (Karpinska et al., 2018). In the movie "ms01" between 13s and 22s there are two cloud void appearances. Motion of the void in the homogeneous cloud field resembles motion of a worm. Movie "ms02" presents cloudy and clear air mixing at the cloud edges.

There were a few series of cloud void images collected with various laser-camera settings on the two experimental days. The best quality series, made in the morning of the 27th, was chosen for void size analysis. For the series of 17 photos selected for analysis, there were four in which voids were not clear enough to be accounted for. In the remaining 13 photos 27 voids were identified. Each one's size was manually determined. In the case of a round void, the diameter was taken as the
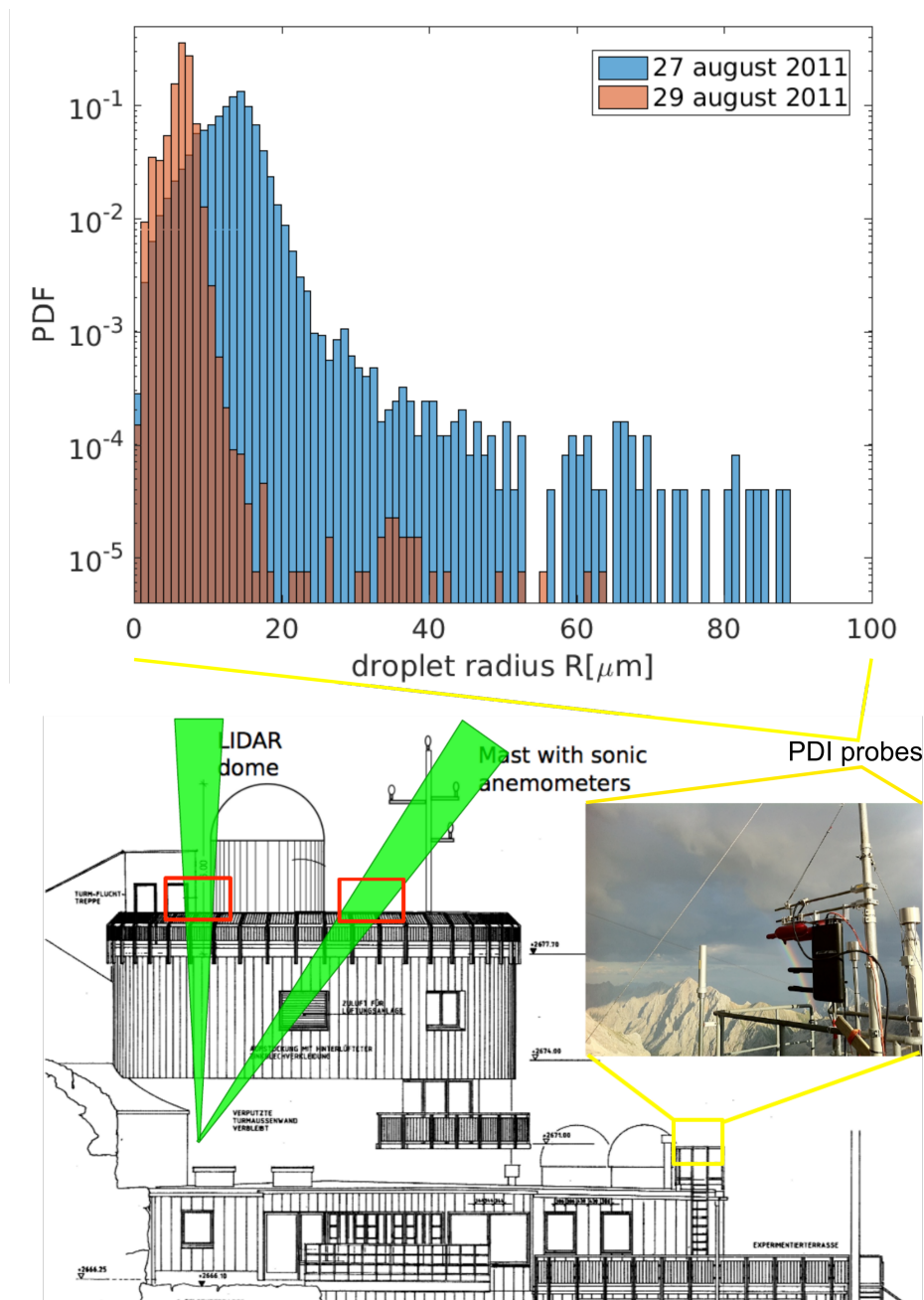
Figure 2. Droplet size distribution measured with a PDI probe (top) and the arrangement of instruments at the measurement site (bottom).

size; in a case of flattened or ellipsoidal void, the maximal chord was taken. The typical void diameter was estimated to be 3.5±1 cm; the maximal, 12±4 cm; the minimal, 1±0.5 cm. Images from the analyzed series from the morning of August 27th showing examples of objects identified as voids are presented in the panel a) of Fig. 1. voids captured on the 29th of August

Table 1. Properties of turbulence and cloud droplets during observation periods.

	August 27th	August 29th
Energy dissipation rate ϵ [m^2/s^3]	0.055	0.070
Kolmogorov length scale η [mm]	0.50	0.47
Mean droplet radius R [μm]	12.9 ± 4.8	6.4 ± 1.5
Sauter mean radius R_{32} [μm]	18.1	7.3
Stokes number St (mean)	0.126	0.035
Stokes number St_{32} (Sauter)	0.247	0.045
Sedimentation parameter Sv	0.676	0.172
Froude number Fr	0.431	0.470
Number density n [cm^{-3}]	56 ± 47	no data

were not analyzed due to the large uncertainty resulting from the unknown geometry of the camera-laser set-up. The general experimental observation was that the voids were smaller then those on August 27th. Definitive experimental verification of the cloud void origin is not possible on the basis of collected data only; however, in next sections, we argue that void creation due to inertia of droplets present inside vortex tubes is highly probable.

5 3   Motion of Heavy, Inertial Particles in the Vortex Tube Model

To address theoretically the issue of cloud void origin, we follow the concept of the polydisperse inertial droplet population response to a coherent vortex pattern. In this section we take the first step on this track presenting relevant features of single droplet trajectory in the chosen vortex tube model. A population of particles is assumed to form a dilute collection of material points, heavy and inertial, displaced by gravity force and viscous force (Stokes drag) only. Burgers vortex is used as a model

10   of a vortex tube. The z-axis in the cylindrical coordinate system (r, φ, z) is aligned with the vortex axis. Its velocity field $\boldsymbol{v}$ is determined by two parameters: circulation Γ and stretching strength γ:

$$\boldsymbol{v} = -\frac{\gamma}{2}r\hat{e}_r + \frac{\Gamma}{2\pi r}\left(1 - e^{-\frac{r^2}{2\delta^2}}\right)\hat{e}_\varphi + \gamma z\hat{e}_z, \tag{2}$$

where $\delta = \sqrt{2\nu/\gamma}$ is the vortex core size and ν denotes the kinematic viscosity. A particle's equation of motion is as follows:

$$\ddot{\boldsymbol{r}} = \frac{1}{\tau_p}\left(\boldsymbol{v} - \dot{\boldsymbol{r}}\right) + \boldsymbol{g}, \tag{3}$$

15   where τ_p is the particle relaxation time and $\boldsymbol{g} = -g\left(\sin\theta\hat{e}_y + \cos\theta\hat{e}_z\right)$ is gravitational acceleration inclined by the angle $\theta \in [0, 90^o]$ with respect to the vortex axis.

The analysis of single droplet motion in projection on a plane (r, φ) perpendicular to the vortex axis (henceforth called 2D
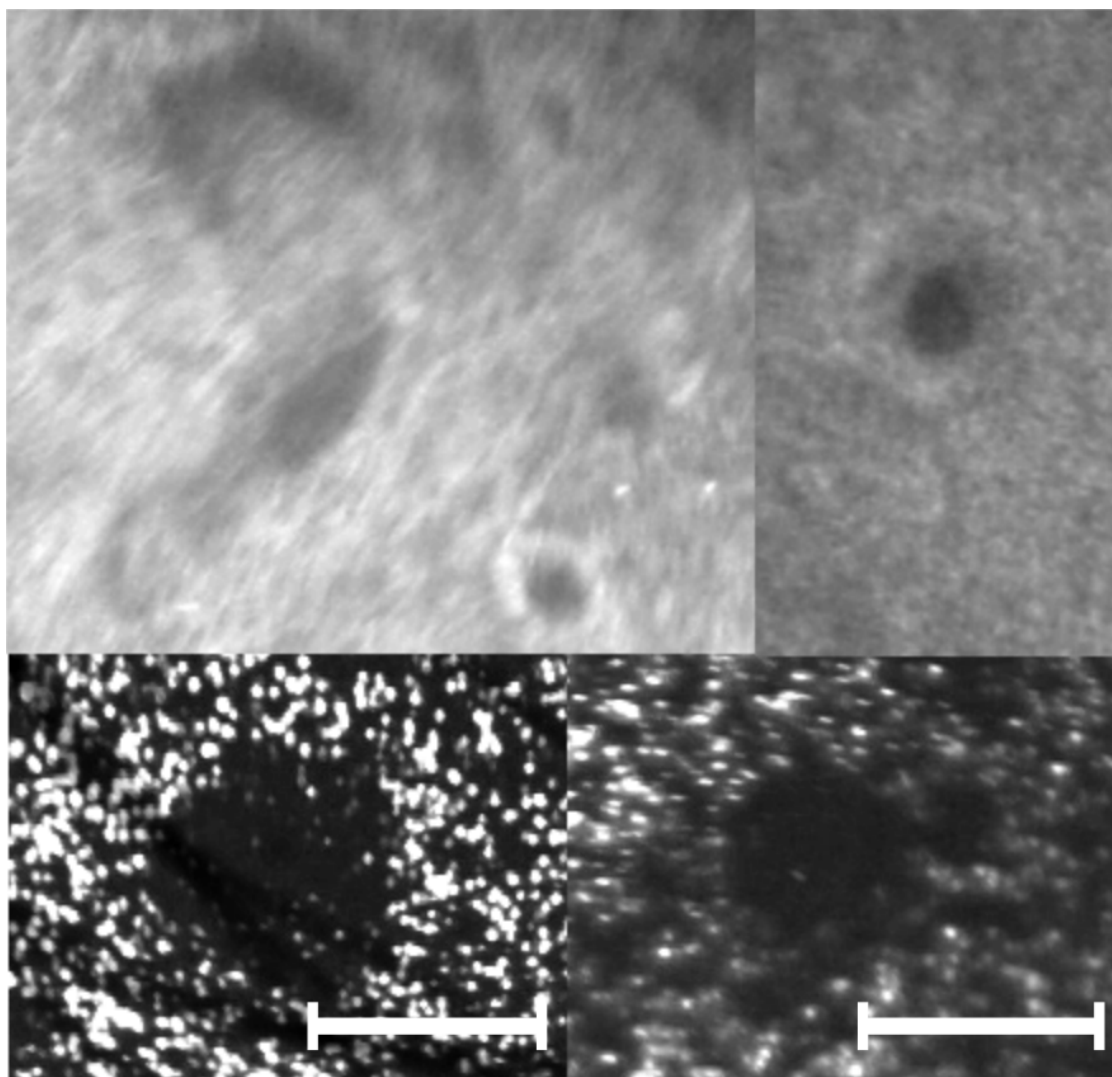
Figure 3. Example close-ups of variously shaped cloud voids observed at the UFS station with different camera-laser configurations. 5 cm long segment is shown to represent spatial scale assumed in the void size calculation.

space) was conducted by Marcu et al. (1995) and is summarized below. The behavior of a droplet inside the vortex depends on a set of six parameters $\{\Gamma, \gamma, \theta, \tau_p, g, \nu\}$. The nondimensionalization of the equations leads to Eq. 4 and gives a set of dimensionless parameters $\{St, Sv, \theta, A\}$:

$$\begin{cases} \ddot{r}^* - r^* \dot{\varphi}^{*2} = -St^{-1}\left(Ar^* + \dot{r}^* + Sv\sin\varphi\right) \\ 2\dot{r}^*\dot{\varphi}^* + r^*\ddot{\varphi}^* = St^{-1}\left(\frac{1}{2\pi r^*}(1 - e^{-\frac{r^{*2}}{2}}) - r^*\dot{\varphi}^* - Sv\cos\varphi\right) \\ \ddot{z}^* = St^{-1}\left(Az - \dot{z}^* - Sv\cot\theta\right) \end{cases} \quad . \tag{4}$$

Henceforth, dimensionless variables are denoted by $*$. Stokes number St was calculated with the use of the characteristic timescale of the Burgers vortex flow, which is the vortex core rotation time $\tau_f = \delta^2 \Gamma^{-1}$, so $St = \tau_p \tau_f^{-1} = \tau_p \Gamma \delta^{-2}$. The sedimentation parameter Sv is a ratio of τ_f to the timescale of sedimentation through the vortex: $Sv = \tau_f \tau_g^{-1} = \delta g \tau_p \sin\theta \Gamma^{-1}$. It

5   characterizes motion in a plane perpendicular to the vortex axis. The last quantity $A = \nu \Gamma^{-1}$ is the strain parameter. It is worth mentioning that the ratio of Stokes number to the sedimentation parameter, called Froude number $Fr = St Sv^{-1}$, is a measure of the influence of gravitational force on the droplet motion. In the limit of a large Froude number, gravity is considered negligible.

10   The solutions of the above equations have several different attractors in 2D space (valid for 3D case without gravity or with gravity parallel to the vortex axis). For every particle of a given radius a stable, circular periodic orbit exists if $St < St_{cr} = 16\pi^2 A$. For $St \geq St_{cr}$, there exists a stable equilibrium point positioned on the vortex axis. A radius of the periodic orbit satisfies the equation:

$$r^{*2} \sqrt{A/St} - \left[1 - \exp\left(-r^{*2}/2\right)\right]/2\pi = 0. \tag{5}$$

15   Nonparallel alignment of the gravity vector and vortex axis ($\theta \neq 0$) destroys the axial symmetry of the system and introduces the presence of other attractors, such as limit cycles and equilibrium points outside the axis.

For a nonzero θ, every particle always has equilibrium points in 2D space. Positions of these points are determined by Sv and A. They can be obtained by solving the equation for the radial component r^*:

$$20 \quad r^* A \sqrt{1 + \left(\frac{1 - \exp\left(\frac{-r^{*2}}{2}\right)}{2\pi A r^{*2}}\right)^2} = Sv. \tag{6}$$

Now, let $f_A(r^*)$ be the left hand side of Eq. 6. A plot of this function for a given A is called a equilibrium curve (see Fig.2 in Marcu et al. (1995)). It is easy to find that $f_A(0) = 0$ and $\lim_{r^* \to \infty} f_A(r^*) = \infty$. Moreover, there exists a critical value $A_{cr} = 0.02176$ for which bifurcation from one unique solution (for $A \geq A_{cr}$) to maximally three solutions (for $A < A_{cr}$) occurs.

25   For $A \geq A_{cr}$ the equilibrium curve is a monotonically increasing function so there is exactly one r^{ast} solution for every Sv value. For $A < A_{cr}$ the equilibrium curve always has one maximum at r^*_{max} and one minimum at r^*_{min}. The inflection point at $A = A_{cr}$ on the equilibrium curve, which lies at $r^*_i = 2.1866$, restricts values of r^*_{max} from above, and values of r^*_{min} from below. Consequently, for $Sv < f_A(r^*_{min})$ and for $Sv > f_A(r^*_{max})$, there is only one solution. For $Sv = f_A(r^*_{min})$ and for $Sv = f_A(r^*_{max})$, there are two solutions. For $f_A(r^*_{min}) < Sv < f_A(r^*_{max})$, there are three solutions.

Table 2. Stability conditions of particle equilibrium points present in the Burgers vortex with respect to vortex strain parameter A and dimensionless distance from the vortex axis r^*. A_t, $\varphi(r^*)$, r_s^*, r_{min}^* and r_{max}^* defined in the text body.

	$\leq r_s^*$	(r_s^*, r_{max}^*)	$[r_{max}^*, r_{min}^*)$	$\geq r_{min}^*$
$A < A_t$	unstable for $St > A/|\phi(r_0^*)|$	stable	partly unstable	stable
$A \geq A_t$			stable	

The stability of the solution r_0^* is governed by the function $\phi(r_0^*)$ (defined in Marcu et al. (1995)). The exact condition depends on the sign of $\phi(r_0^*)$. Since the function has only one zero at $r_s^* = 1.585201$, there are two cases. For small radii ($r_0^* < r_s^*$), the equilibrium is stable if:

$$\frac{St}{A} \leq \frac{1}{|\phi(r_0^*)|}. \tag{7}$$

For greater radii ($r_0^* > r_s^*$), the condition for stability depends explicitly only on A:

$$A \geq \sqrt{\phi(r_0^*)}. \tag{8}$$

The equilibrium point satisfying the first type of the condition was shown to be a focus; the second type, a node. Different scenarios of particle motion determined by above stability conditions were shown in Fig.4 in Marcu et al. (1995). Fig. 4 here presents a simplified illustration of one of the scenarios: three equilibrium points, unstable point near the axis, stable point far from the axis, and droplets rotating around the vortex center.

Particle motion along the vortex axis is separated from the motion 2D space and can be found analytically. It is determined by stretching outflow drag and gravity. As a consequence, as found in (Karpinska and Malinowski, 2014), position z shows an exponential dependence on time. Every droplet has one unstable equilibrium point $z_0^* = SvA^{-1}\cot\theta$.

4 Conditions for Void Creation

The results described above were used to formulate the following hypothesis concerning conditions of void creation: a majority of the polydisperse droplets in cloud must have an unstable equilibrium point close to the axis $r_0^* < r_s^*$ (leading to a limit cycle or periodic orbit). Attraction by a coexisting stable equilibrium point far from the axis $r_0^* > r_{min}^*$ should not influence their trajectories in a certain volume around the void. Hence, the analysis of the equilibrium point stability conditions has to be expanded by putting emphasis on the dependence on strain parameter A. The results were described in detail below and are summarised in Table 2.

The stability conditions change for $A_t = \max_{r_0^*}\left(\sqrt{\varphi(r_0^*)}\right) \approx 0.01917$. It is the maximum of right-hand side in Inequality 8 obtained numerically. $A > A_t$ always satisfies then the condition expressed by 8. The term "partly unstable" in the table refers to the following: In the range of $r_0^* \in [r_{max}^*, r_{min}^*)$, for a given A, only a small fraction of the total range (near points r_{max}^* and
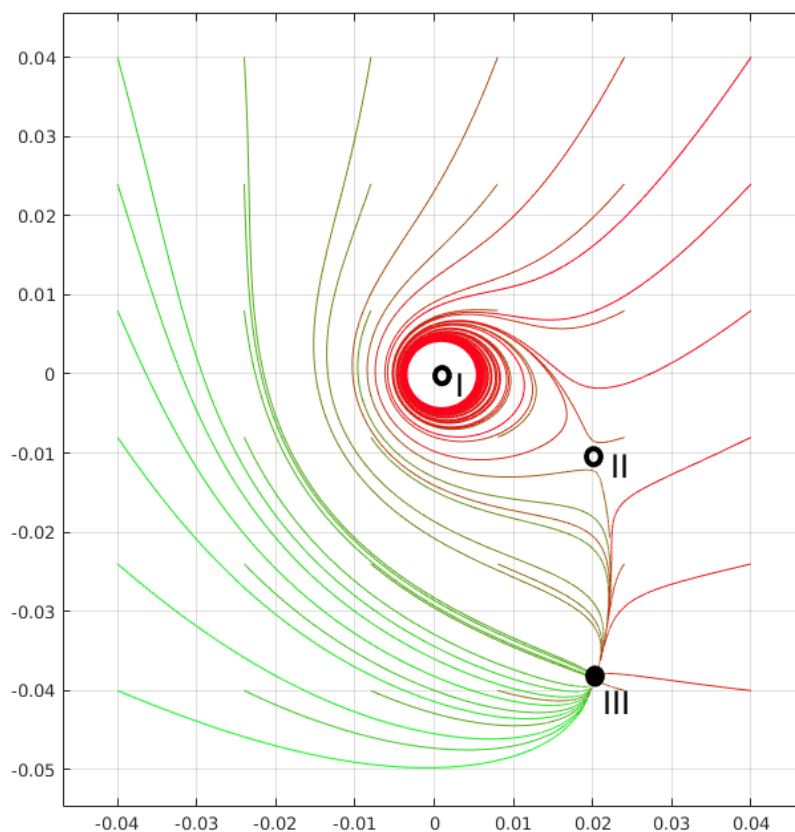
Figure 4. Example illustration of droplet trajectories in 2D space (projection on a plane perpendicular to the vortex axis). Particle trajectories (color lines) show the presence of three equilibrium points marked with black dots: I - unstable near vortex axis, II - unstable middle distance point, III - stable point far from the axis. Some droplets rotate around the vortex core on various orbits, some of these orbits may correspond to limit cycles. Different attraction regions can be noticed.

r^*_{min}) is stable. This range grows with increasing A. Numerical experiments show, however, that their domain of attraction in the presence of other stable points (at least one exists always) is relatively small.

Obtaining mathematically strict condition for creation of an arbitrary sized void in polydisperse collection of droplets is too complicated to be used directly for comparison with crude experimental results. Thorough analysis of single droplet motion however, can be used to draw approximate conclusions. The obvious statement is that when circulation of the vortex is too small: $A \geq A_{cr}$, the motion of particles is determined mostly by the gravitational force and resembles simple falling through the vortex, but with curved trajectories. In the case $A \leq A_{cr}$ Table 2 indicates that the void can be created if the majority of particles have unstable equillibrium points near the center. Radial position of such a point r^* in the range $r^* \leq r^*_s$ can be approximated using a linearization of Eq. 6:

$$r^* \simeq 4\pi Sv \left(1 + (4\pi A)^2\right)^{-\frac{1}{2}}. \tag{9}$$

The function determining stability condition (Eq. 7) can be approximated in this range as follows: $\phi(r^*_0) \simeq -(1 - r^*_0/r^*_s) * \left(16\pi^2\right)^{-1}$. At $r^* = 0$ it has the same form as obtained for the case without gravity in Marcu et al. (1995). Further stability analysis requires introducing a new dimnensionless parameter B:

$$B = \underbrace{\frac{r^*_s}{2^8\pi^3}}_{const} \frac{\nu^2}{g\sin\theta\delta^3}. \tag{10}$$

The condition for unstable points near the axis splits in parts. The first part concerns only vortex parameters and the second part particle sizes. The first part requires that strain parameter A must be small enough (and consequently circulation large enough):

$$A < A_{max} = 2^{-1/6}B^{1/3} + O(B^2). \tag{11}$$

The second part demands that particle Stokes number falls within the range $(St_1, St_1 + \Delta St)$ (results shown to the leading term order in A):

$$\begin{aligned} St_1 &= 2^4\pi^2 A + O(A^4) \\ \Delta St &= 2^6\pi^2 BA^{-2} + O(A^0) \end{aligned}. \tag{12}$$

The following rough conclusions can be drawn from the above relations:

- There is a threshold (minimal) value of circulation needed for void creation. It increases with gravity influence ($g\sin\theta$) and vortex size δ.

- The greater the circulation the smaller particles have their unstable points near the axis.

- The range of particles having unstable points near the axis increases with increasing circulation and decreases with increasing gravity influence and vortex size δ.

Building up on these results it may be concluded that it is harder to observe voids created by horizontally aligned vortices than

5 vertically aligned ones and the harder with increasing range of particle sizes.

5   Vortex Tube Model Parameter Ranges

Using the above theoretical conclusions a careful search for vortex model parameter values was carried out to verify whether observed cloud voids could be attributed to the presence of vortex tubes. The search was made using simplified numerical

10 simulations of droplet trajectories in vortices of varying circulation and orientation, and with droplets of varying sizes. The results are described below. Premises found in the literature described in the introduction were used for making the assumption that the proportionality constant in Eq. 1 is in the range $m \in [3.5, 24]$. The relation between the vortex stretching parameter and the Kolmogorov length $\gamma = 2\nu\delta^{-2} = 2\nu(m\eta)^{-2}$ leads then to $\gamma \in [0.21, 8.35]s^{-1}$. Particle and vortex constants and parameters were chosen to match those of water droplets in the cloudy air and for the remaining discussion particles are called droplets.

15 To estimate the range of the strain parameter, the following educated guess was made. void creation demands that most of the droplets in 2D space circle the vortex axis at a certain distance. Approximation of the droplet trajectory curvature radius by the periodic orbit radius described by Eq. 5 seems reasonable. Figure 5 presents contours of periodic orbit radius solutions as a function of vortex parameters. Contours were selected to match experimental void radii and are labeled in centimeters. Three droplet sizes R were chosen to represent the experimental range for August 27th (see Table 1). Colored areas correspond to

20 the periodic orbit existence condition, $St < St_{cr}$. This leads to the limitation of the strain parameter for further analysis to a range $A \in [5 \cdot 10^{-5}, 8 \cdot 10^{-3}]$. It can be noticed that $A < A_{cr}$, which according to the analysis in Sec. 4 means it is outside the purely gravitational regime, with the possibility of particles having one unstable equilibrium point near the vortex axis and/or one stable equilibrium point far from the axis.

6   Numerical Simulations

25 The hypothesis of cloud void appearance was verified by numerical simulations. To imitate processes occurring in real vortex tubes in clouds and examine the effect exerted on a droplet field by the presence of a vortex, a cylinder-shaped domain was chosen. At $t = 0$, the domain was filled uniformly with a given number concentration n of droplets. Droplets leaving the simulation domain were constantly removed, and no interaction between droplets was imposed. Initial positions of the new droplets appearing in the domain at $t > 0$ were randomized on the cylinder surface to obtain conditions "outside the cylinder" of homo-

30 geneous spatial distribution with the same n. The initial velocity of these droplets was adjusted to the radial inflow velocity. The simulation domain size was chosen to be capable of showing phenomena at scales larger than standard experimental cloud void size, such that $Z = 12$ cm long and $D = 5$ cm in radius. Sensitivity to different values of D was examined, and no significant
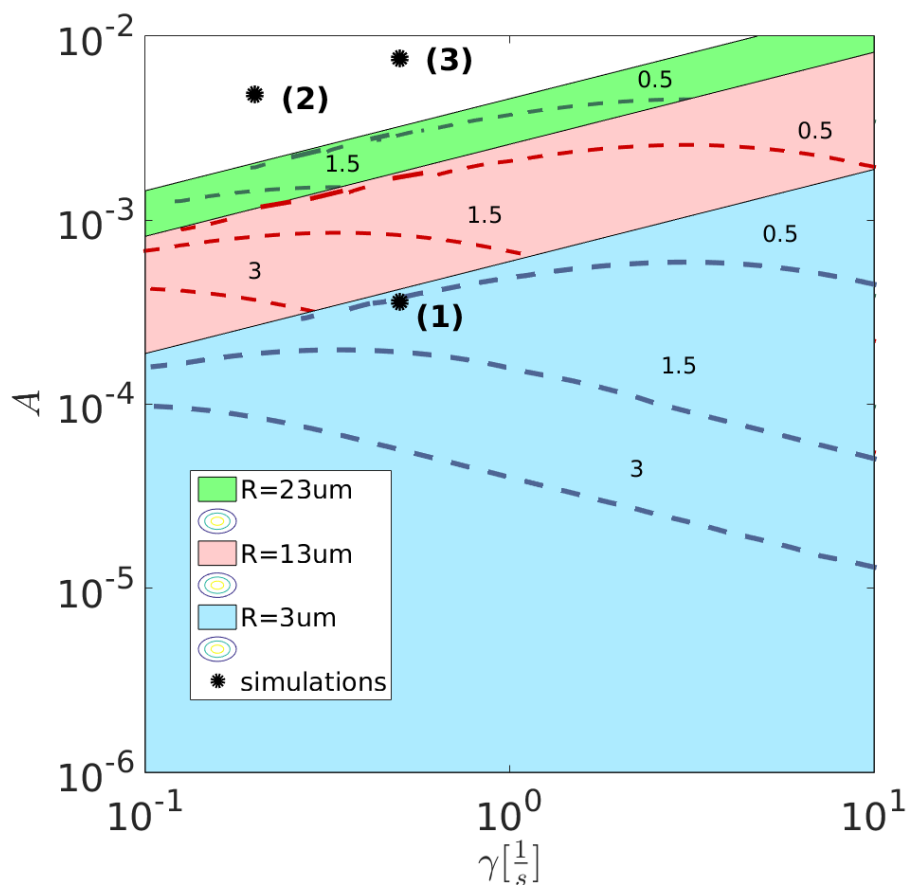
Figure 5. Contour plot of stable periodic 2D orbit radius for droplets of radii $R = 3, 13, 23 \ \mu m$ covering the experimental range on August 27th. Selected ranges of vortex parameters: stretching γ and strain A are in x an y axes, respectively. Overlapping (blue on a top, then pink and green) colored surfaces match regions in which stable periodic 2D orbit exist for a given droplet radius. Dashed contours match experimental void radii labeled in cm. Black points represent parameters set for simulations as described in the next section.

Table 3. Sets of vortex and particle parameters chosen for numerical simulation. St, Sv, Fr are mean values. Only sets 1) and 2) give the visual effects of the cloud void.

	$\gamma\,[\frac{1}{s}]$	$\delta\,[cm]$	θ	A	A_{max}	St	Sv	Fr
1)	0.5	0.78	$\pi/8$	0.00036	0.003	1.45	0.0014	31.82
2)	0.2	1.2	$\pi/4$	0.0048	0.0016	0.045	0.055	0.91
3)	0.5	0.78	$\pi/4$	0.0076	0.0024	0.068	0.057	1.096

dependence was noticed. An almost constant droplet number within the domain was obtained in the course of the simulation. A semi-Gaussian distribution of droplet radii cut off at $R = 1.5\mu$m was chosen for simulations to match the experimental values from the 27th of August (see Table 1). Since droplets do not interact and results do not depend on droplet concentration, $n = 10$ cm^{-3} or $n = 20\,\mathrm{cm}^{-3}$ was chosen in order to minimize computational time. After 5 s to 8 s each simulation reached stationarity.

Experimental images of cloud voids were obtained with monochromatic green laser light scattered by spherical droplets at a certain forward angle (see Sec. 2). A large variability in visibility of individual droplets marginally differing in radius could, due to Mie scattering properties, influence observed patterns resulting from voids. To reflect these effects in the post-processing of simulation results, a $40°$ scattering angle was used. Visualizations in Fig.5 show droplets scaled by both size and color brightness in order to represent scattered light intensity. The Mie scattering algorithm used is described in (Raffel et al., 1998).

Two simulations, 1) and 2), with parameters described in Table 3 result in the presence of a round or close to round void around the vortex axis. Simulation 3) does not show anything close to void creation or any other persistent pattern formation. The three simulation cases were chosen to indicate that the theoretical prediction presented in Fig.5 is just an approximate tool to manage a complex problem.: although parameter sets 2) and 3) are on the "no-void" side, case 2 gives visible impression of a void. This is further confirmed by noticing that value of A in case 2) is greater than A_{max}. It means that even in the case of droplets being attracted by their stable points near the axis it is possible that the attraction is weak. Just a few seconds of motion resembles rotation around an unstable point which is able to create a void.

Figure 6 presents a 3D picture (panels a and b) with a 2D cross-section (c and d) at the last, quasi stationary stage of simulations 1) and 2). In the database (Karpinska et al., 2018) one may find animations from the simulations both in 2D and 3D. Animations "ms03" and "ms04" correspond to set 1), "ms05" and "ms06" to set 2), "ms07" and "ms08" to set 3).

To qualitatively present the droplet spatial structure in a void, all droplets were divided into five bins equal in droplet number. Number concentration n with respect to the distance from the vortex axis r was plotted in panels e and f of Fig. 6 with different shading colors representing contributions from different size groups. A homogeneous distribution of droplets in space would give a horizontal line. Sorting and clustering effects of the vortex presence caused by attraction of stable equilibrium points and limit cycles are clearly seen. Line plots in the same panel present droplet mean radius $\langle R \rangle$ and droplet mean visible radius $\langle S \rangle$ (scaled according to Mie scattering) with respect to the distance from vortex axis r. In the absence of sorting and
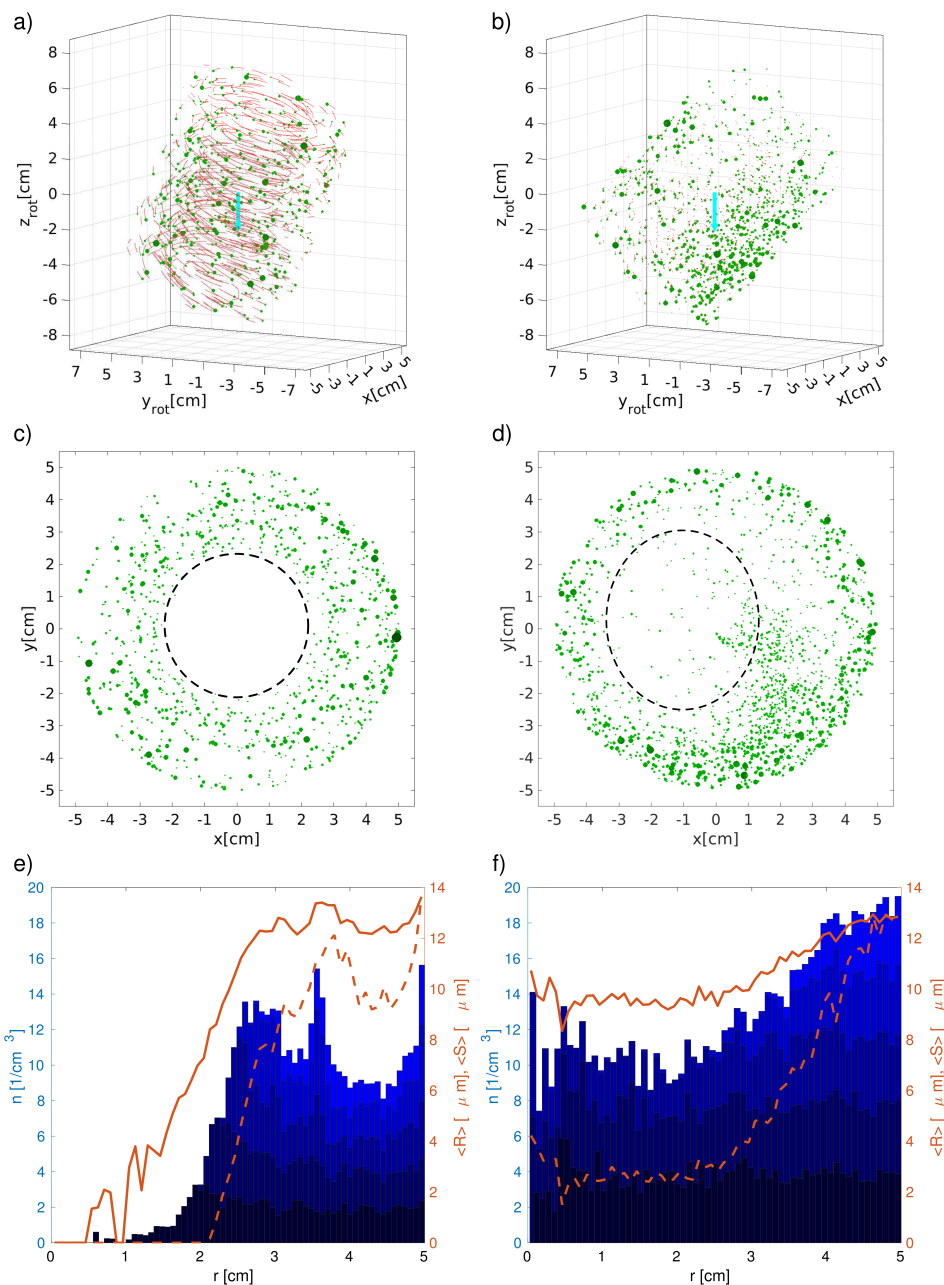
Figure 6. Positions of droplets in simulations 1) (left side) and 2) (right side) as described in Table 3 in perspective view (panels a and b) and in 2 cm-thick central slice projected on a plane perpendicular to the vortex axis (panels c and d). The blue arrow shows the direction of gravity. In panels a-d, droplet color and size are proportional to the Mie scattering intensity. The red lines in panels a and b reflect the last $\Delta t = 0.06\ s$ of the droplet trajectory (for clarity every 10th droplet drawn). The gray dashed circles reflect the approximate shape and size of the visible void in the droplet field. Panels e) and f) present the number concentration of droplets n with different blue shading colors representing the contribution from different size groups - left axis, droplet mean real radius (solid line); right axis - mean visible radius (dashed line), all with respect to the distance from the vortex axis r. **15**

clustering, the plots would approach horizontal lines. Their actual shape demonstrates a strong influence of droplet sorting on strengthening the visible void effect. On the basis of the real droplet radius plot, the radii of the voids can be estimated as ∼ 0-1.5 cm; however, the visible void radii are rather ∼ 2-2.5 cm, which seems close to the experimental values and is on the order of the Burgers vortex core size δ.

In summary, there are two possible factors together creating the visible effect of the void. The first one is droplet dynamics: the majority of the droplets move on helical trajectories, being attracted in 2D space by the limit cycle or by a stable point near the axis. The largest ones may be slowly attracted by their equilibrium point far from the vortex axis in 2D space, but in the course of attraction they circle around the axis. At the same time, a significant ratio of the characteristic timescale of motion in the plane perpendicular to vortex axis with respect to motion along the vortex axis is needed. The second factor is the visibility of droplets in the laser sheet: variation of Mie scattering intensities with droplet radius is large, so the smallest droplets moving towards their stable equilibrium point near the vortex axis may not be visible in the laser sheet picture. This strengthens visible void creation for $A > A_{max}$ as in the simulation set 2). In effect, there may exist a wide range of vortex parameters that can result in the visual effect of a void of a certain radius for a given droplet size distribution.

7   Discussion and Conclusions

Visualizations of cloud droplets by means of laser sheet photography performed at the Schneefernerhaus observatory revealed the presence of voids - holes in the form of curved elongated cylinders with a radius of a few centimeters (see the movie in the supplementary materials). The possibility of such cloud voids or "Swiss cheese" cuts in clouds was suggested by former studies of the Stokes motion of cloud droplets in idealized Burgers or line vortices. Using information on cloud droplet size distributions and turbulence parameters collected in the course of observations, as well as literature discussions on vortex tubes in turbulent flows, we have shown that the cloud voids observed under the experimental conditions were very likely a result of the presence of relatively thin yet long vortex tubes. Approximate theoretical conditions of void creation on primarily vortex tube circulation and other vortex and droplet parameters were proposed. The calculations are consistent with the observation that voids are present under some conditions and not under others. Comparison of the modeled and observed voids led to the conclusion that properties of the Mie scattering of laser sheet light have to be accounted for to reproduce the proper size and shape of the observed cloud voids.

This finding, if confirmed in clouds far from the atmospheric surface layer, might help to better understand the effect of high Reynolds number turbulence on clustering, size sorting and probably collisions of cloud droplets. In the literature, several perspectives on this problem were presented: the centrifuge mechanism for small St particles in the dissipation range in Maxey (1987); the sweep-stick mechanism described in Coleman and Vassilicos (2009) correlating fluid zero-acceleration points with droplet clusters; caustics - points in space of multiple valued particle velocity, as summed up in Gustavsson and Mehlig (2016) - or the sling effect, analogous to caustics, presented in Falkovich and Pumir (2007). Considering droplet motion within a single vortex, representative of coherent dissipative structures expected to exist in turbulent flows, as in the present

paper, is a strong simplification in comparison to the cited works. However, the research conducted for non-sedimenting particles in Ravichandran and Govindarajan (2015), Deepu et al. (2017) suggests that fixed point attraction and caustics formed by limit cycle attraction strongly increase the clustering and collisions of particles near single and multiple vortices. This fact should become very distinct motivation for investing in both experimental and research aiming at thorough quantitative characterization of cloud void events.

Code and data availability. Numerical simulation code available on demand. Data repository containing experimental movies and animations of simulations is retrieved from: https://www.researchgate.net/publication/328429794_Data_supporting_the_paper_Turbulence_induced_cloud_voids_observation_and_interpretation.

Author contributions. Raymond Shaw, Holger Siebert and Eberhard Bodenschatz designed the experiment. Szymon Malinowski formulated the aim for theoretical and numerical analysis. Steffen Risius, Tina Shmeissner, Raymond Shaw, Holger Siebert, Hengdong Xi, Haitao Xu Jonathan Bodenschatz and Eberhard Bodenschatz provided resources and carried out the experiment. Tina Shmeissner, Steffen Risius, Haitao Xu, Eberhard Bodenshatz maintained and synthesized experimental data. Szymon Malinowski and Eberhard Bodenschatz acquired financial support. Katarzyna Karpińska and Szymon Malinowski developed numerical model. Katarzyna Karpińska analysed the experimental data, conducted theoretical analysis, designed and implemented the code for numerical analysis, conducted validation and verification of numerical results, wrote the original draft of the paper. Katarzyna Karpińska and Steffen Riusius provided visualisation of the results. Szymon Malinowski was responsible for supervision. Katarzyna Karpinska, Szymon Malinowski, Jakub Nowak, Steffen Riusius, Raymond Shaw and Holger Siebert edited the original draft to prepare it for submission.

Competing interests. No competing interest are present.

Acknowledgements. We are grateful to Mr. Markus Neumann and the staff at UFS for their technical help at UFS and the Bavarian Umweltministerium for the financial support of the station. Financial support from Max Planck Society, Deutsche Forschungsgemeinschaft (DFG) through the SPP 1276 Metström, the EU COST Action MP0806 Particles in Turbulence, Polish National Science Centre (grant 2013/08/A/ST10/00291) and through the US National Science Foundation (NSF grant AGS-1026123) are gratefully acknowledged. We thank Marta Wacławczyk and Liang Ping Wang for the comments on the manuscript.

References

Belin, F., Moisy, F., Tabeling, P., and Willaime, H.: Worms in a turbulence experiment, from hot wire time series, in: Fundamental Problematic
    Issues in Turbulence, Trends in Mathematics, p. 129–140, 1999.

Biferale, L., Scagliarini, A., and Toschi, F.: On the measurement of vortex filament lifetime statistics in turbulence, Physics Letters A, 276,
    115–121, 2000.

Bodenschatz, E., Malinowski, S. P., Shaw, R. A., and Stratmann, F.: Can We Understand Clouds Without Turbulence?, Science, 327, 970–971,
    https://doi.org/10.1126/science.1185138, http://science.sciencemag.org/content/327/5968/970, 2010.

Chuang, P. Y., Saw, E. W., Small, J. D., Shaw, R. A., Sipperley, C. M., Payne, G. A., and Bachalo, W. D.: Airborne Phase Doppler Interferome-
    try for Cloud Microphysical Measurements, Aerosol Science and Technology, 42, 685–703, https://doi.org/10.1080/02786820802232956,
    http://dx.doi.org/10.1080/02786820802232956, 2008.

Coleman, S. W. and Vassilicos, J. C.: A unified sweep-stick mechanism to explain particle clustering in two- and three-dimensional ho-
    mogeneous, isotropic turbulence, Physics of Fluids, 21, 113 301, https://doi.org/10.1063/1.3257638, https://doi.org/10.1063/1.3257638,
    2009.

Deepu, P., Ravichandran, S., and Govindarajan, R.: Caustics-induced coalescence of small droplets near a vortex, Physical Reviev Fluids, 2,
    024 305, https://doi.org/10.1103/PhysRevFluids.2.024305, https://link.aps.org/doi/10.1103/PhysRevFluids.2.024305, 2017.

Falkovich, G. and Pumir, A.: Sling Effect in Collisions of Water Droplets in Turbulent Clouds, Journal of the Atmospheric Sciences, 64,
    4497–4505, https://doi.org/10.1175/2007JAS2371.1, 2007.

Gerber, H., Malinowski, S. P., and Jonsson, H.: Evaporative and Radiative Cooling in POST Stratocumulus, Journal of the Atmospheric
    Sciences, 73, 3877–3884, https://doi.org/10.1175/JAS-D-16-0023.1, https://doi.org/10.1175/JAS-D-16-0023.1, 2016.

Gustavsson, K. and Mehlig, B.: Statistical models for spatial patterns of heavy particles in turbulence, Advances in Physics, 65, 1–57, 2016.

Hill, R. J.: Geometric collision rates and trajectories of cloud droplets falling into a Burgers vortex, Physics of Fluids, 17, 037 103,
    https://doi.org/10.1063/1.1858191, 2005.

Jimenez, J. and Wray, A.: On the characteristics of vortex filaments in isotropic turbulence, Journal of Fluid Mechanics, 373, 255–285, 1998.

Jiménez, J., Wray, A., Rogallo, R., and Saffman, P.: The structure of intense vorticity in isotropic turbulence, Journal of Fluid Mechanics,
    255, 65–90, 1993.

Karpinska, K. and Malinowski, S.: Towards better understanding of preferential concentration in clouds: droplets in small vortices, in:
    American Meteorological Society 14th Conference on Cloud Physics, 2014.

Karpinska, K., Bodenschatz, J. F., Malinowski, S. P., Nowak, J. L., Risius, S., Schmeissner, T., A.Shaw, R., Siebert, H., Xi, H., Xu, H., and
    Bodenschatz, E.: Data supporting the paper "Turbulence induced cloud voids: observation and interpretation"., 2018.

Marcu, B., Meiburg, E., and Newton, P. K.: Dynamics of heavy particles in a burgers vortex, Physics of Fluids, 7, 400–410, 1995.

Markowicz, K., Bajer, K., and Malinowski, S. P.: Influence of small-scale turbulence structures on the concentration of cloud droplets, in:
    13th Conference on Clouds and Precipitation, IAMAP, 2000.

Maxey, M. R.: The gravitational settling of aerosol particles in homogeneous turbulence and random flow fields, Journal of Fluid Mechanics,
    174, 441–465, https://doi.org/10.1017/S0022112087000193, 1987.

Maxey, M. R. and Corrsin, S.: Gravitational Settling of Aerosol Particles in Randomly Oriented Cellular Flow Fields, Journal of the Atmo-
    spheric Sciences, 43, 1112–1134, https://doi.org/10.1175/1520-0469(1986)043<1112:GSOAPI>2.0.CO;2, 1986.

Moisy, F. and Jimenez, J.: Geometry and clustering of intense structures in isotropic turbulence, Journal of Fluid Mechanics, 513, 111–133, https://doi.org/10.1017/S0022112004009802, 2004.

5   Mouri, H., Hori, A., and Kawashima, Y.: Vortex tubes in velocity fields of laboratory isotropic turbulence, Physics Letters A, 276, 115–121, 2000.

Neu, J. C.: The dynamics of stretched vortices, Journal of Fluid Mechanics, 143, 253–276, https://doi.org/10.1017/S0022112084001348, https://www.cambridge.org/core/article/dynamics-of-stretched-vortices/1783CBAF5D397FD30CD90BB137533477, 1984.

Pirozzoli, S.: On the velocity and dissipation signature of vortex tubes in isotropic turbulence, Physica D Nonlinear Phenomena, 241, 10   202–207, 2012.

Raffel, M., Willert, C., and Kompenhans, J.: Particle Image Velocimetry: A Practical Guide, Engineering online library, Springer Berlin Heidelberg, https://books.google.pl/books?id=dopRAAAAMAAJ, 1998.

Ravichandran, S. and Govindarajan, R.: Caustics and clustering in the vicinity of a vortex, Physics of Fluids, 27, 033 305, https://doi.org/10.1063/1.4916583, https://doi.org/10.1063/1.4916583, 2015.

15   Risius, S., Xu, H., Di Lorenzo, F., Xi, H., Siebert, H., Shaw, R. A., and Bodenschatz, E.: Schneefernerhaus as a mountain research station for clouds and turbulence, Atmospheric Measurement Techniques, 8, 3209–3218, https://doi.org/10.5194/amt-8-3209-2015, http://www.atmos-meas-tech.net/8/3209/2015, 2015.

Shaw, R. A.: Supersaturation Intermittency in Turbulent Clouds, Journal of the Atmospheric Sciences, 57, 3452–3456, https://doi.org/10.1175/1520-0469(2000)057<3452:SIITC>2.0.CO;2, 2000.

20   Shaw, R. A., Reade, W. C., Collins, L. R., and Verlinde, J.: Preferential Concentration of Cloud Droplets by Turbulence: Effects on the Early Evolution of Cumulus Cloud Droplet Spectra, Journal of the Atmospheric Sciences, 55, 1965–1976, https://doi.org/10.1175/1520-0469(1998)055<1965:PCOCDB>2.0.CO;2, 1998.

Siebert, H., Shaw, R. A., Ditas, J., Schmeissner, T., Malinowski, S. P., Bodenschatz, E., and Xu, H.: High-resolution measurement of cloud microphysics and turbulence at a mountaintop station, Atmospheric Measurement Techniques, 8, 3219–3228, https://doi.org/10.5194/amt-25   8-3219-2015, http://www.atmos-meas-tech.net/8/3219/2015, 2015.

Tanahashi, M., Fujibayashi, K., and Miyauchi, T.: Fine Scale Eddy Cluster and Energy Cascade in Homogeneous Isotropic Turbulence, Proceedeings of IUTAM Symposium on Computational Physics and New Perspectives in Turbulence, 4, 67–72, 2008.

Tennekes, H. and Woods, J. D.: Coalescence in a weakly turbulent cloud, Quarterly Journal of the Royal Meteorological Society, 99, 758–763, https://doi.org/10.1002/qj.49709942215, http://dx.doi.org/10.1002/qj.49709942215, 1973.

Warhaft, Z.: Passive Scalars in Turbulent Flows, Annual Review of Fluid Mechanics, 32, 203–240, https://doi.org/10.1146/annurev.fluid.32.1.203, https://doi.org/10.1146/annurev.fluid.32.1.203, 2000.